Structural basis for neutralization of SARS-CoV-2 and SARS-CoV by a potent therapeutic antibody

Authors: Zhe Lv[1,8$], Yong-Qiang Deng[2$], Qing Ye[2,$], Lei Cao[1$], Chun-Yun Sun[3$], Changfa Fan[4$], Weijin Huang[5], Shihui Sun[2], Yao Sun[1], Ling Zhu[1], Qi Chen[2], Nan Wang[1,8], Jianhui Nie[5], Zhen Cui[1,8], Dandan Zhu[1], Neil Shaw[1], Xiao-Feng Li[2], Qianqian Li[5], Liangzhi Xie[3,6,7]*, Youchun Wang[5]*, Zihe Rao[1]*, Cheng-Feng Qin[2]* and Xiangxi Wang[1,8]*

Affiliation:

[1] CAS Key Laboratory of Infection and Immunity, National Laboratory of Macromolecules, Institute of Biophysics, Chinese Academy of Sciences, Beijing 100101, China

[2] State Key Laboratory of Pathogen and Biosecurity, Institute of Microbiology and Epidemiology, Academy of Military Medical Sciences, Beijing, China.

[3] Beijing Protein and Antibody R&D Engineering Center, Sinocelltech Ltd., Beijing 100176, China

[4] Division of Animal Model Research, Institute for Laboratory Animal Resources, National Institutes for Food and Drug Control (NIFDC), Beijing 102629, China;

[5] Division of HIV/AIDS and Sex-Transmitted Virus Vaccines, Institute for Biological Product Control, National Institutes for Food and Drug Control (NIFDC), Beijing 102629, China

[6] Beijing Antibody Research Key Laboratory, Sino Biological Inc., Building 9, Jing Dong Bei Technology Park, No.18 Ke Chuang 10th St, BDA, Beijing, 100176, China

[7] Cell Culture Engineering Center, Chinese Academy of Medical Sciences & Peking Union Medical College, Beijing 100005, China

[8] University of Chinese Academy of Sciences, Beijing 100049, China

*Correspondence to: X.W. (Email: xiangxi@ibp.ac.cn) or C.F.Q. (Email: qincf@bmi.ac.cn) or Y.W. (Email: wangyc@nifdc.org.cn) or L.X. (Email: liangzhi@yahoo.com) or Z.R. (Email: raozh@tsinghua.edu.cn)

[$] These authors contributed equally to this work.

Abstract:

The COVID-19 pandemic caused by the SARS-CoV-2 virus has resulted in an unprecedented public health crisis. There are no approved vaccines or therapeutics for treating COVID-19. Here we reported a humanized monoclonal antibody, H014, efficiently neutralizes SARS-CoV-2 and SARS-CoV pseudoviruses as well as authentic SARS-CoV-2 at *nM* level by engaging the S receptor binding domain (RBD). Importantly, H014 administration reduced SARS-CoV-2 titers in the infected lungs and prevented pulmonary pathology in hACE2 mouse model. Cryo-EM characterization of the SARS-CoV-2 S trimer in complex with the H014 Fab fragment unveiled a novel conformational epitope, which is only accessible when the RBD is in open conformation. Biochemical, cellular, virological and structural studies demonstrated that H014 prevents attachment of SARS-CoV-2 to its host cell receptors. Epitope analysis of available neutralizing antibodies against SARS-CoV and SARS-CoV-2 uncover broad cross-protective epitopes. Our results highlight a key role for antibody-based therapeutic interventions in the treatment of COVID-19.

One sentence summary

A potent neutralizing antibody conferred protection against SARS-CoV-2 in an hACE2 humanized mouse model by sterically blocking the interaction of the virus with its receptor.

63 **Main Text:** The coronavirus disease 2019 (COVID-19) pandemic had afflicted >7
64 million people in more than 200 countries/regions, resulting in 400,000 deaths as of 8
65 June, according to the World Health Organization. The etiological agent of this
66 pandemic is the newly emerging coronavirus, severe acute respiratory syndrome
67 coronavirus 2 (SARS-CoV-2), which, together with the closely related SARS-CoV
68 belongs to the lineage B of the genus *Betacoronavirus* in the *Coronaviridae* family (*1*).
69 Sharing an amino acid sequence identity of ~80% in the envelope-located spike (S)
70 glycoprotein, both SARS-CoV-2 and SARS-CoV utilize human angiotensin
71 converting enzyme 2 (hACE2) to enter into host cells. Cellular entry is achieved by
72 the homotrimeric S mediated virus-receptor engagement through the receptor binding
73 domain (RBD) followed by virus-host membrane fusion (*1, 2*). Abrogation of this
74 crucial role played by the S-protein in the establishment of an infection is the main
75 goal of neutralizing antibodies and the focus of therapeutic interventions as well as
76 vaccine design (*3-6*). Several previously characterized SARS-CoV neutralizing
77 antibodies (NAbs) were demonstrated to exhibit very limited neutralization activities
78 against SARS-CoV-2 (*7-9*). Among these, CR3022, a weakly neutralizing antibody
79 against SARS-CoV, is tight binding, but non-neutralizing for SARS-CoV-2,
80 indicative of possible conformational differences in the neutralizing epitopes (*9*).
81 More recent studies have reported two SARS-CoV neutralizing antibodies, 47D11
82 and S309, that have been shown to neutralize SARS-CoV-2 as well (*10, 11*),
83 suggesting that broad cross-neutralizing epitopes exist within lineage B. Convalescent
84 plasma containing SARS-CoV-2 neutralizing antibodies (NAbs) have been shown to
85 confer clear protection in COVID-19 patients (*12, 13*), yet gaps in our knowledge
86 concerning the immunogenic features and key epitopes of SARS-CoV-2, have
87 hampered the development of effective immuno-therapeutics against the virus.
88
89 The RBDs of SARS-CoV and SARS-CoV-2 have an amino-acid sequence identity of
90 around 75%, raising the possibility that RBD-targeting cross-neutralizing NAbs could
91 be possibly identified. Using phage display technique, we constructed an antibody
92 library which was generated from RNAs extracted from peripheral lymphocytes of
93 mice immunized with recombinant SARS-CoV RBD. SARS-CoV-2 RBD was used as

94 the target for screening the phage antibody library for potential hits. Antibodies
95 showing tight binding for SARS-CoV-2 RBD were further propagated as chimeric
96 antibodies and tested for neutralizing activities using a vesicular stomatitis virus
97 (VSV) based pseudotyping system (fig. S1) (*14*). Among the antibodies tested, clone
98 014 which showed potent neutralizing activity against SARS-CoV-2 pseudovirus was
99 humanized, named as H014. To evaluate the binding affinities, real-time association
100 and dissociation of H014 binding to either SARS-CoV-2 RBD or SARS-CoV RBD
101 were monitored using the OCTET system (Fortebio). Both H014 Ig G and Fab
102 fragments exhibited tight binding to both RBDs with comparable binding affinities at
103 sub-nM levels for SARS-CoV-2 RBD and SARS-CoV RBD, respectively (Fig. 1A
104 and fig. S2). Pseudovirus neutralization assays revealed that H014 has potent
105 neutralizing activities: a 50% neutralizing concentration value (IC_{50}) of 3 nM and 1
106 nM against SARS-CoV-2 and SARS-CoV pseudoviruses, respectively (Fig. 1B).
107 Plaque-reduction neutralization test (PRNT) conducted against an authentic
108 SARS-CoV-2 strain (BetaCoV/Beijing/AMMS01/2020) verified the neutralizing
109 activities with an IC_{50} of 38 nM, 10-fold lower than those observed in the
110 pseudotyping system (Fig. 1C). We next sought to assess *in vivo* protection efficacy of
111 H014 in our previously established human ACE2 (hACE2) humanized mouse model
112 that was sensitized to SARS-CoV-2 infection (*15*). In this model, as a result of hACE2
113 expression on lung cells, SARS-CoV-2 gains entry into the lungs and replicates as in a
114 human disease, exhibiting lung pathology at 5 days post infection (dpi).
115 hACE2-humanized mice were treated by intraperitoneal injection of H014 at 50
116 mg/kg either 4 hours after (1 dose, therapeutic) or 12 hours before and 4 hours after (2
117 doses, prophylactic plus therapeutic) intranasal infection with 5×10^5 PFU of
118 SARS-CoV-2 (BetaCoV/Beijing /AMMS01/2020). All challenged animals were
119 sacrificed at day 5. While the viral loads in the lungs of the PBS group (control)
120 surged to ~10^7 RNA copies/g at day 5 (Fig. 1D), remarkably, in the prophylactic and
121 prophylactic plus therapeutic groups, H014 treatment resulted in a ~10-fold and
122 100-fold reduction of viral titers in the lungs at day 5, respectively (Fig. 1D). Lung
123 pathology analysis showed that SARS-CoV-2 caused mild interstitial pneumonia

124 characterized by inflammatory cell infiltration, alveolar septal thickening and
125 distinctive vascular system injury upon PBS treatment. In contrast, no obvious lesions
126 of alveolar epithelial cells or focal hemorrhage were observed in the lung sections
127 from mice that received H014 treatment (Fig. 1E), indicative of a potential therapeutic
128 role for H014 in curing COVID-19.

129

130 The overall structure of SARS-CoV-2 S trimer resembles those of SARS-CoV and
131 other coronaviruses. Each monomer of the S protein is composed of two functional
132 subunits. The S1 subunit binds the host cell receptor, while the S2 subunit mediates
133 fusion of the viral membrane with the host cell membrane (*2, 16*). The four domains
134 within S1 include N-terminal domain (NTD), RBD and two subdomains (SD1 and
135 SD2) where the latter are positioned adjacent to the S1/S2 cleavage site. Hinge-like
136 movements of the RBD give rise to two distinct conformational states referred to as
137 the "close" and "open", where close corresponds to the receptor-inaccessible state and
138 open corresponds to the receptor-accessible state, which is supposed to be metastable
139 (*17-20*). Cryo-EM characterization of the stabilized SARS-CoV-2 S ectodomain in
140 complex with the H014 Fab fragment revealed that the complex adopts three distinct
141 conformational states, corresponding to one RBD open + two RBDs closed (state 1),
142 two RBDs open + one RBD closed (state 2) and all three open RBDs (state 3) (Fig.
143 2A). Interestingly, structure of the completely closed (state 4) SARS-CoV-2 S trimer
144 without any Fab bound was also observed during 3D classification of the cryo-EM
145 data, albeit in the presence of excessive Fab, suggesting that the binding sites of H014
146 are exposed through protein "breathing" followed by a stochastic RBD movement
147 (Fig. 2A). We determined asymmetric cryo-EM reconstructions of the 4 states at 3.4 –
148 3.6 Å (figs. S3-S6 and table S1). However, the electron potential maps for binding
149 interface between RBD and H014 are relatively weak due to conformational
150 heterogeneity. To solve this problem, focusing classification and refinement by using
151 a "block-based" reconstruction approach were performed to further improve the local
152 resolution up to 3.9 Å, enabling reliable analysis of the interaction mode (fig. S5-S6).
153 Detailed analysis of the interactions between H014 and S was done using the binding
154 interface structure.

155 H014 recognizes a conformational epitope on one side of the open RBD, only
156 involving protein/protein contacts, distinct from the receptor-binding motif (RBM)
157 (Fig. 2B). The H014 paratope constitutes all six complementary determining region
158 (CDR) loops (CDRL1-3 and CDRH1-3) and unusual the heavy-chain frame work
159 (HF-R, residues 58-65) that forge tight interactions with the RBD, resulting in a
160 buried area of ~1,000 $Å^2$ (Fig. 2C). Variable domains of the light-chain and
161 heavy-chain contribute ~32% and 68% of the buried surface area, respectively,
162 through hydrophobic and hydrophilic contacts. The H014 epitope is composed of 21
163 residues, primarily locating in the α2-β2-η2 (residues 368-386), η3 (residues 405-408,
164 411-413), α4 (residue 439) and η4 (residues 503) regions, which construct a cavity on
165 one side of the RBD (Fig. 2B, 2D and fig. S7). The 12-residue long CDRH3 inserts
166 into this cavity and the hydrophobic residues (YDPYYVM) enriched CDRH3
167 contacts the η3 and edge of the five-stranded β-sheet (β2) region of the RBD (Fig.
168 2D). Tight bindings between the RBD and H014 are primarily due to extensive
169 hydrophobic interactions contributed by two patches: one formed by F54 from
170 CDRH2, Y101 from CDRH3 and A411, P412 and Y508 of the RBD and the other
171 composed of Y49 from CDRL2, P103, Y104, Y105 from CDRH3 and V407, V503
172 and Y508 of the RBD (Fig. 2E and table S2). Additionally, hydrophilic contacts from
173 CDRH1 and HF-R further enhance the RBD-H014 interactions, leading to an
174 extremely high binding affinity at sub nM level at temperatures of 25 °C or 37 °C (Fig.
175 2E and fig. S8). Residues comprising the epitope are mostly conserved with 3
176 single-site mutants (R408I, N439K and V503F) in this region among currently
177 circulating SARS-CoV-2 strains reported (fig. S9). In addition, a number of
178 SARS-CoV-2 isolates bear a common mutation V367F in the RBD (*21*), which lies
179 adjacent to the major epitope patch α2-β2-η2. Constructs of the recombinant RBD
180 harboring point mutations of above residues and other reported substitutions exhibited
181 an indistinguishable binding affinity to H014 (fig. S10), suggesting that H014 may
182 exhibit broad neutralization activities against SARS-CoV-2 strains currently
183 circulating worldwide. Out of the 21 residues in the H014 epitope, 17 (81 %) are
184 identical between SARS-CoV-2 and SARS-CoV (fig. S9), which explains the
185 cross-reactivity and comparable binding affinities.

186 To investigate whether H014 interferes with the binding of RBDs of SARS-CoV-2 or
187 SARS-CoV to ACE2, we performed competitive binding assays at both protein and
188 cellular levels. The enzyme-linked immunosorbent assay (ELISA) indicated that
189 H014 was able to compete with recombinant ACE2 for binding to RBDs of
190 SARS-CoV-2 and SARS-CoV with EC_{50} values of 0.7 nM and 5 nM, respectively
191 (Fig. 3A). Additionally, H014 efficiently blocked both the attachment of SARS-CoV-2
192 RBD to ACE2 expressing 293T cells and the binding of recombinant ACE2 to
193 SARS-CoV-2 S expressing 293T cells (Fig. 3B). To verify its potential full occlusion
194 on trimeric S, we conducted two sets of surface plasmon resonance (SPR) assays by
195 exposing the trimeric S to H014 first and then to ACE2 or the other way around. As
196 expected, binding of H014 completely blocked the attachment of ACE2 to trimeric S.
197 Moreover, ACE2 could be displaced from trimeric S and replaced by H014 (Fig. 3C).
198 To further verify these results in a cell-based viral infection model, real time RT-PCR
199 analysis was carried out to quantify the amount of virus remaining on the host cell
200 surface, which were exposed to antibodies pre- or post-virus attachment to cells at
201 4 °C. H014 efficiently prevented attachment of SARS-CoV-2 to the cell surface in a
202 dose-dependent manner and the viral particles that had already bound to the cell
203 surface could be partially stripped by H014 (Fig. 3D). Superimposition of the
204 structure of the H014-SARS-CoV-2 trimeric S complex over the ACE2-SARS-CoV-2
205 RBD complex structure revealed clashes between the ACE2 and H014, arising out of
206 an overlap of the regions belonging to the binding sites located at the apical helix (η4)
207 of the RBD (Fig. 3E). This observation differs substantially from those of most known
208 SARS RBD-targeted antibody complexes, where the antibodies directly recognize the
209 RBM (*22-25*). Thus, the ability of H014 to prevent SARS-CoV-2 from attaching to
210 host cells can be attributed to steric clashes with ACE2.
211
212 Similar to the RBM, the H014 epitope is only accessible in the open state, indicative
213 of a role akin to the RBM – involving dynamic interferences in interactions with host
214 cells. Our structures together with previously reported coronavirus S structures, not
215 including human coronavirus HKU1 (*20*), have observed the breathing of the S1
216 subunit, that mediates the transition between “close” and “open” conformation (Fig.

217 4A) (*2, 9, 20*). In contrast to the hinge-like movement of the RBD observed in most
218 structures, the conformational transition from "close" to "open" observed in our
219 structures mainly involves two steps of rotations: 1) counterclockwise movement of
220 SD1 by ~25° encircling the hinge point (at residue 320); 2) the RBD rotates itself
221 counterclockwise by ~60° (Fig. 4B). These conformational rotations of the SD1 and
222 RBD at proximal points relay an amplified alteration at the distal end, leading to
223 opening up of adequate space for the binding of H014 or ACE2 (Fig. 4B).
224 Ambiguously, the special conformational transition observed in our complex
225 structures results from the engagement of H014 or a synergistic movement of the SD1
226 and RBD.
227
228 Humoral immunity is essential for protection against coronavirus infections and
229 passive immunization of convalescent plasma has been demonstrated to be effective
230 in treating SARS and COVID-19 (*12, 26*). A number of SARS-CoV specific
231 neutralizing antibodies including m396, 80R and F26G19, have been previously
232 reported to engage primarily the RBM core (residues 484-492 in SARS-CoV)
233 provided that the RBD is in open conformation (Fig. 4C and 4D) (*24, 27, 28*).
234 Unexpectedly, none of these antibodies has so far demonstrated impressive
235 neutralizing activity against SARS-CoV-2 (*7, 8*). S230, a SARS-CoV neutralizing
236 antibody that functionally mimics receptor attachment and promotes membrane fusion,
237 despite requiring an open state of the RBD as well, recognizes a small patch at the top
238 of the RBM (Fig. 4C and 4D) (*17*). Recently, two other antibodies (CR3022 and S309)
239 originating from the memory B cells of SARS survivors in 2003, demonstrated strong
240 binding to SARS-CoV-2 (*9, 10*). Surprisingly, CR3022 failed to neutralize
241 SARS-CoV-2 *in vitro*, which could be attributed to the fact that CR3022 binds a
242 cryptic epitope, which is distal from the RBD and is only accessible when at least two
243 RBDs are in the open state. Furthermore, CR3022 does not compete with ACE2 for
244 binding to the RBD (Fig. 4C and 4D) (*9*). By contrast, S309, a more recently reported
245 neutralizing mAb against both SARS-CoV and SARS-CoV-2, recognizes a conserved
246 glycan-containing epitope accessible in both the open and closed states of SARS-CoV
247 and SARS-CoV-2 RBDs (*10*). The neutralization mechanism of S309 does not depend

248 on direct blocking of receptor binding, but it induces antibody-dependent cell
249 cytotoxicity (ADCC) and antibody-dependent cellular phagocytosis (ADCP). We
250 reported a potent therapeutic antibody H014, which can cross-neutralize SARS-CoV-2
251 and SARS-CoV infections by blocking attachment of the virus to the host cell (Fig. 3).
252 Distinct from other antibodies, H014 binds one full side of the RBD, spanning from
253 the proximal η2 to the distal edge of the RBM and possesses partially overlapping
254 epitopes with SARS-CoV specific antibodies like m392, 80R, F26G19, CR3022 and
255 S309 (Fig. 4C and 4D). Although both SARS-CoV and SARS-CoV-2 utilize ACE2 to
256 enter host cells, high sequence variations in the RBM and local conformational
257 rearrangements at the distal end of the RBM from the two viruses have been observed
258 (*8*). These probably lead to the failure of some antibodies, especially those targeting
259 the RBM of SARS-CoV, in cross-binding and cross-neutralizing SARS-CoV-2. Three
260 cross-reactive antibodies (CR3022, S309 and H014) recognize more conserved
261 epitopes located beyond the RBM, amongst which the CR3022 epitope is most distant
262 from the RBM (Fig. 4C and 4D), suggesting a possible reason for its inability to
263 neutralize SARS-CoV-2. H014 binds more conserved epitopes, some of which are in
264 close proximity to the RBM, rendering it effective in cross-neutralizing lineage B
265 viruses. Additionally, antibodies recognizing more conserved patches beyond the
266 RBM would function synergistically with antibodies targeting the RBM to enhance
267 neutralization activities, which could mitigate the risk of viral escape. The molecular
268 features of H014 epitopes unveiled in this study facilitate the discovery of broad
269 cross-neutralizing epitopes within lineage B and pose interesting targets for
270 structure-based rational vaccine design. Our studies also highlight the promise of
271 antibody-based therapeutic interventions for the treatment of COVID-19.
272
273
274
275
276
277 **References and Notes:**

278 1. P. Zhou, X. L. Yang *et al.*, A pneumonia outbreak associated with a new coronavirus of
279 probable bat origin. *nature* **579**, 270-273 (2020); published online EpubMar

(10.1038/s41586-020-2012-7).

2. A. C. Walls, Y. J. Park *et al.*, Structure, Function, and Antigenicity of the SARS-CoV-2 Spike Glycoprotein. *Cell* **181**, 281-292 e286 (2020); published online EpubApr 16 (S0092-8674(20)30262-2).

3. L. B. : Qiang Gao, Haiyan Mao, Lin Wang, Kangwei Xu, Rapid development of an inactivated vaccine for SARS-CoV-2. *Science*, (2020).

4. D. Corti, J. Zhao *et al.*, Prophylactic and postexposure efficacy of a potent human monoclonal antibody against MERS coronavirus. *Proc Natl Acad Sci U S A* **112**, 10473-10478 (2015); published online EpubAug 18 (10.1073/pnas.1510199112).

5. J. Pallesen, N. Wang *et al.*, Immunogenicity and structures of a rationally designed prefusion MERS-CoV spike antigen. *Proc Natl Acad Sci U S A* **114**, E7348-E7357 (2017); published online EpubAug 29 (10.1073/pnas.1707304114).

6. A. C. Walls, M. A. Tortorici *et al.*, Glycan shield and epitope masking of a coronavirus spike protein observed by cryo-electron microscopy. *Nat Struct Mol Biol* **23**, 899-905 (2016); published online EpubOct (10.1038/nsmb.3293).

7. X. Tian, C. Li *et al.*, Potent binding of 2019 novel coronavirus spike protein by a SARS coronavirus-specific human monoclonal antibody. *Emerg Microbes Infect* **9**, 382-385 (2020)10.1080/22221751.2020.1729069).

8. J. Lan, J. Ge *et al.*, Structure of the SARS-CoV-2 spike receptor-binding domain bound to the ACE2 receptor. *nature*, (2020); published online EpubMar 30 (10.1038/s41586-020-2180-5).

9. M. Yuan, N. C. Wu *et al.*, A highly conserved cryptic epitope in the receptor-binding domains of SARS-CoV-2 and SARS-CoV. *Science*, (2020); published online EpubApr 3 (10.1126/science.abb7269).

10. M. B. Young-Jun Park, Alexandra C. Walls, M. Alejandra Tortorici, Michael S. Diamond, Katja Fink, David Veesler, Davide Corti, Structural and functional analysis of a potent sarbecovirus neutralizing antibody. *BioRxiv*, (2020)doi: https://doi.org/10.1101/2020.04.07.023903).

11. C. Wang, W. Li *et al.*, A human monoclonal antibody blocking SARS-CoV-2 infection. *Nature communications* **11**, 2251 (2020); published online EpubMay 4 (10.1038/s41467-020-16256-y).

12. A. Casadevall, L. A. Pirofski, The convalescent sera option for containing COVID-19. *J Clin Invest* **130**, 1545-1548 (2020); published online EpubApr 1 (10.1172/JCI138003).

13. C. Shen, Z. Wang *et al.*, Treatment of 5 Critically Ill Patients With COVID-19 With Convalescent Plasma. *Jama*, (2020); published online EpubMar 27 (10.1001/jama.2020.4783).

14. J. Nie, Q. Li *et al.*, Establishment and validation of a pseudovirus neutralization assay for SARS-CoV-2. *Emerg Microbes Infect* **9**, 680-686 (2020); published online EpubDec (10.1080/22221751.2020.1743767).

15. Q. C. Shi-Hui Sun, Hong-Jing Gu, Guan Yang, Yan-Xiao Wang, Chang-Fa Fan, Yu-Sen Zhou, Cheng-Feng Qin, You-Chun Wang, A mouse model of SARS-CoV-2 infection and pathogenesis. *BioRxiv*, (2020).

16. D. Wrapp, N. Wang *et al.*, Cryo-EM structure of the 2019-nCoV spike in the prefusion conformation. *Science* **367**, 1260-1263 (2020); published online EpubMar 13

(10.1126/science.abb2507).
17. A. C. Walls, X. Xiong *et al.*, Unexpected Receptor Functional Mimicry Elucidates Activation of Coronavirus Fusion. *Cell* **176**, 1026-1039 e1015 (2019); published online EpubFeb 21 (10.1016/j.cell.2018.12.028).
18. M. Gui, W. Song *et al.*, Cryo-electron microscopy structures of the SARS-CoV spike glycoprotein reveal a prerequisite conformational state for receptor binding. *Cell Res* **27**, 119-129 (2017); published online EpubJan (10.1038/cr.2016.152).
19. Y. Yuan, D. Cao *et al.*, Cryo-EM structures of MERS-CoV and SARS-CoV spike glycoproteins reveal the dynamic receptor binding domains. *Nature communications* **8**, 15092 (2017); published online EpubApr 10 (10.1038/ncomms15092).
20. R. N. Kirchdoerfer, C. A. Cottrell *et al.*, Pre-fusion structure of a human coronavirus spike protein. *nature* **531**, 118-121 (2016); published online EpubMar 3 (10.1038/nature17200).
21. Z. Z. Junxian Ou, Jing Zhang, Wendong Lan, Shan Zhao, Jianguo Wu, Donald Seto, Gong Zhang, Qiwei Zhang, RBD mutations from circulating SARS-CoV-2 strains enhance the structural stability and human ACE2 affinity of the spike protein. *BioRxiv*, (2020).
22. J. ter Meulen, E. N. van den Brink *et al.*, Human monoclonal antibody combination against SARS coronavirus: synergy and coverage of escape mutants. *PLoS Med* **3**, e237 (2006); published online EpubJul (10.1371/journal.pmed.0030237).
23. J. Sui, W. Li *et al.*, Potent neutralization of severe acute respiratory syndrome (SARS) coronavirus by a human mAb to S1 protein that blocks receptor association. *Proc Natl Acad Sci U S A* **101**, 2536-2541 (2004); published online EpubFeb 24 (10.1073/pnas.0307140101).
24. E. N. van den Brink, J. Ter Meulen *et al.*, Molecular and biological characterization of human monoclonal antibodies binding to the spike and nucleocapsid proteins of severe acute respiratory syndrome coronavirus. *J Virol* **79**, 1635-1644 (2005); published online EpubFeb (10.1128/JVI.79.3.1635-1644.2005).
25. J. D. Berry, S. Jones *et al.*, Development and characterisation of neutralising monoclonal antibody to the SARS-coronavirus. *J Virol Methods* **120**, 87-96 (2004); published online EpubSep 1 (10.1016/j.jviromet.2004.04.009).
26. A. C. Cunningham, H. P. Goh *et al.*, Treatment of COVID-19: old tricks for new challenges. *Crit Care* **24**, 91 (2020); published online EpubMar 16 (10.1186/s13054-020-2818-6).
27. P. Prabakaran, J. Gan *et al.*, Structure of severe acute respiratory syndrome coronavirus receptor-binding domain complexed with neutralizing antibody. *J Biol Chem* **281**, 15829-15836 (2006); published online EpubJun 9 (10.1074/jbc.M600697200).
28. W. C. Hwang, Y. Lin *et al.*, Structural basis of neutralization by a human anti-severe acute respiratory syndrome spike protein antibody, 80R. *J Biol Chem* **281**, 34610-34616 (2006); published online EpubNov 10 (10.1074/jbc.M603275200).
29. K. Zhang, Gctf: Real-time CTF determination and correction. *J Struct Biol* **193**, 1-12 (2016); published online EpubJan (10.1016/j.jsb.2015.11.003).
30. S. H. Scheres, Processing of Structurally Heterogeneous Cryo-EM Data in RELION. *Methods enzymol* **579**, 125-157 (2016)10.1016/bs.mie.2016.04.012).
31. S. H. Scheres, S. Chen, Prevention of overfitting in cryo-EM structure determination. *Nature methods* **9**, 853-854 (2012).

32. Y. Yang, P. Yang *et al.*, Architecture of the herpesvirus genome-packaging complex and implications for DNA translocation. *Protein & cell* **11**, 339-351 (2020); published online EpubMay (10.1007/s13238-020-00710-0).
33. N. Wang, D. Zhao *et al.*, Architecture of African swine fever virus and implications for viral assembly. *Science* **366**, 640-644 (2019); published online EpubNov 1 (10.1126/science.aaz1439).
34. N. Wang, W. Chen *et al.*, Structures of the portal vertex reveal essential protein-protein interactions for Herpesvirus assembly and maturation. *Protein & cell* **11**, 366-373 (2020); published online EpubMay (10.1007/s13238-020-00711-z).
35. A. Kucukelbir, F. J. Sigworth *et al.*, Quantifying the local resolution of cryo-EM density maps. *Nature methods* **11**, 63-65 (2014).
36. E. F. Pettersen, T. D. Goddard *et al.*, UCSF Chimera—a visualization system for exploratory research and analysis. *Journal of computational chemistry* **25**, 1605-1612 (2004).
37. A. Brown, F. Long *et al.*, Tools for macromolecular model building and refinement into electron cryo-microscopy reconstructions. *Acta Crystallographica Section D-Structural Biology* **71**, 136-153 (2015); published online EpubJan (10.1107/S1399004714021683).
38. P. V. Afonine, R. W. Grosse-Kunstleve *et al.*, Towards automated crystallographic structure refinement with phenix. refine. *Acta Crystallographica Section D: Biological Crystallography* **68**, 352-367 (2012).
39. V. B. Chen, W. B. Arendall *et al.*, MolProbity: all-atom structure validation for macromolecular crystallography. *Acta Crystallographica Section D: Biological Crystallography* **66**, 12-21 (2010).
40. X. Wang, L. Zhu *et al.*, Potent neutralization of hepatitis A virus reveals a receptor mimic mechanism and the receptor recognition site. *Proc Natl Acad Sci U S A* **114**, 770-775 (2017)
41. M. Larkin, G. Blackshields *et al.*, Clustal W and Clustal X version 2.0. *Bioinformatics* **23**, 2947-2948 (2007).

Acknowledgments: We thank Dr. Xiaojun Huang, Dr. Boling Zhu and Dr. Gang Ji for cryo-EM data collection, the Center for Biological imaging (CBI) in Institute of Biophysics for EM work. Work was supported by the National Key Research and Development Program (2020YFA0707500, 2018YFA0900801), the Strategic Priority Research Program (XDB29010000), National Science and Technology Major Projects of Infectious Disease funds (grants 2017ZX103304402) and Beijing Municipal Science and Technology Project (Z201100005420017). Xiangxi Wang was supported by Ten Thousand Talent Program and the NSFS Innovative Research Group (No. 81921005). Cheng-Feng Qin was supported by the National Science Fund for Distinguished Young Scholar (No. 81925025) and the Innovative Research Group (No. 81621005) from the NSFC, and the Innovation Fund for

Medical Sciences (No.2019-I2M-5-049) from the Chinese Academy of Medical Sciences. “ L.X. and C. S. are inventors on patent application (202010219867.1) submitted by Sinocelltech. Ltd that covers the intellectual property of H014”. **Author contributions**: Zhe.L., Y.D., C.S., Q.Y., L.C., C.F., W.H., Y.S., Q.C., S.S., N.W., D.Z., J.N., Z.C., N.S. and X.L. performed experiments; X.W., C-F.Q, Z.R., L.X. and Y.W. designed the study; all authors analyzed data; and X.W., L.Z., C-F.Q. and Z.R. wrote the manuscript. **Competing interests**: All authors have no competing interests. **Data and materials availability**: Cryo-EM density maps of the *apo* SARS-CoV-2 S trimer, SARS-CoV-2 S trimer in complex with one Fab, SARS-CoV-2 S trimer in complex with two Fabs, SARS-CoV-2 S trimer in complex with three Fabs and binding interface have been deposited at the Electron Microscopy Data Bank with accession codes EMD-30325, EMD-30326, EMD-30332, EMD-30333 and EMD-30331 and related atomic models has been deposited in the protein data bank under accession code 7CAB, 7CAC, 7CAI, 7CAK and 7CAH, respectively.

Figure legends

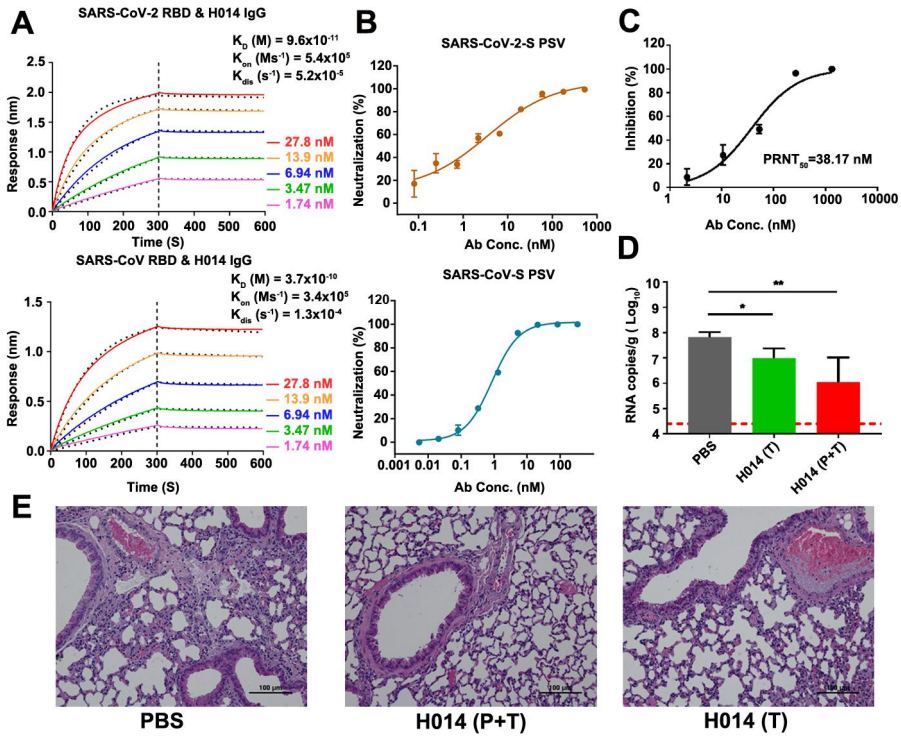

Fig. 1 H014 is a lineage B cross-neutralizing antibody of therapeutic value

(A) Affinity analysis of the binding of H014 to RBD of SARS-CoV-2 and SARS-CoV. Biotinylated RBD proteins of (upper) SARS-CoV-2 or (lower) SARS-CoV were loaded on Octet SA sensor and tested for real-time association and dissociation of the H014 antibody. Global fit curves are shown as black dotted lines. The vertical dashed lines indicate the transition between association and disassociation phases. **(B)** Neutralizing activity of H014 against SARS-CoV-2 and SARS-CoV pseudoviruses (PSV). Serial dilutions of H014 were added to test its neutralizing activity against (upper) SARS-CoV-2 and (lower) SARS-CoV PSV. Neutralizing activities are represented as mean ± SD. Experiments were performed in triplicate. **(C)** *In vitro* neutralization activity of H014 against SARS-CoV-2 by PRNT in Vero cells. Neutralizing activities are represented as mean ± SD. Experiments were performed in duplicates. **(D)** Groups of hACE2 mice that received SARS-CoV-2 challenge were treated intraperitoneally with H014 in two independent experimental settings: 1) a single dose at 4 h post infection (Therapeutic, T); 2) two doses at 12 h before and 4 h post challenge (Prophylactic plus Therapeutic, P+T). Virus titers in the lungs were measured 5 days post

infection (dpi) and are presented as RNA copies per gram of lung tissue. n=7/3/3, respectively. *P<0.05. LOD represents limit of detection. **(E)** Histopathological analysis of lung samples at 5 dpi. Scale bar: 100 μm.

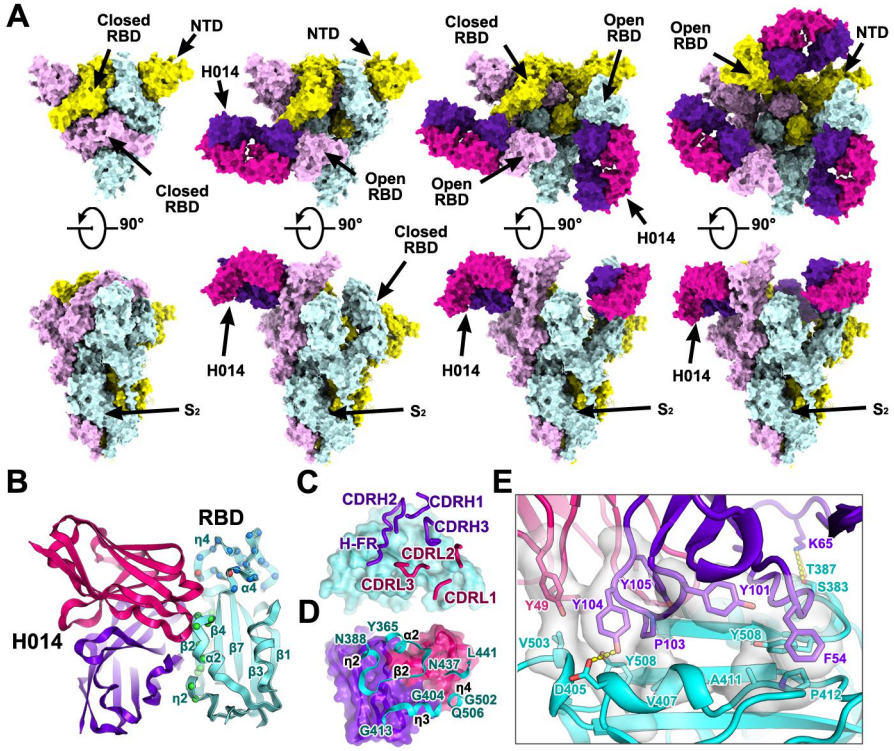

Fig. 2 Cryo-EM structures of the SARS-CoV-2 S trimer in complex with H014

(A) Orthogonal views of SARS-CoV-2 S trimer with three RBDs in the closed state (left), one RBD in the open state and complexed with one H014 Fab (middle), two RBDs in the open state and each complexed with one H014 Fab. NTD: N-terminal domain. All structures are presented as molecular surfaces with different colors for each S monomer (cyan, violet and yellow), and the H014 Fab light (hotpink) and heavy (purpleblue) chains. **(B)** Cartoon representations of the structure of SARS-CoV-2 RBD in complex with H014 Fab with the same color scheme as in Fig. 2A. Residues comprising the H014 epitope and the RBM are shown as spheres and colored in green and blue, respectively. The overlapped residues between the H014 epitope and the RBM are shown in red. **(C)** and **(D)** Interactions between the H014 and SARS-CoV-2 RBD. The CDRs of the H014 that interact with SARS-CoV-2 RBD are displayed as thick tubes over the cyan surface of the RBD **(C)**. The H014 epitope is shown as a cartoon representation over the surface of the RBD **(D)**. **(E)** Details of the interactions between the H014 and SARS-CoV-2 RBD. Some residues involved in the formation of hydrophobic patches and hydrogen

bonds are shown as sticks and labeled. Color scheme is the same as in Fig. 2A.

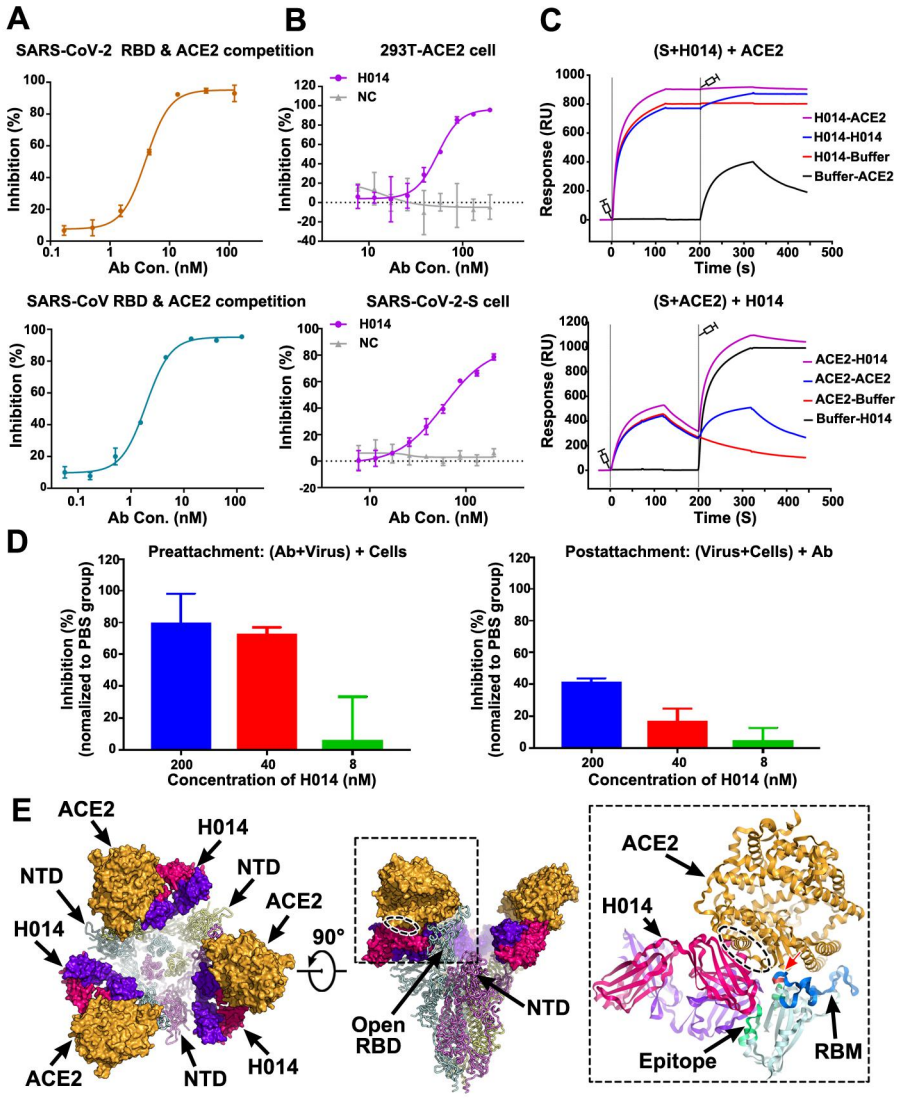

Fig. 3 Mechanism of neutralization of H014

(A) Competitive binding assays by ELISA. Recombinant SARS-CoV-2 (upper) or SARS-CoV (lower) RBD protein was coated on 96-well plates, recombinant ACE2 and serial dilutions of H014 were then added for competitive binding to SARS-CoV-2 or SARS-CoV RBD. Values are mean ± SD. Experiments were performed in triplicate. **(B)** Blocking of SARS-CoV-2 RBD binding to 293T-ACE2 cells by H014 (upper). Recombinant SARS-CoV-2 RBD protein and serially diluted H014 were incubated with ACE2 expressing 293T cells (293T-ACE2) and tested for binding of H014 to 293T-ACE2 cells. Competitive binding of H014 and ACE2 to SARS-CoV-2-S cells (lower). Recombinant ACE2 and serially diluted H014 were incubated with 293T cells expressing SARS-CoV-2 Spike protein (SARS-CoV-2-S)

587 and tested for binding of H014 to SARS-CoV-2-S cells. BSA was used as a
588 negative control (NC). Values are mean ± SD. Experiments were performed in
589 triplicate. **(C)** BIAcore SPR kinetics of competitive binding of H014 and ACE2 to
590 SARS-CoV-2 S trimer. For both panels, SARS-CoV-2 S trimer was loaded onto the
591 sensor. In the upper panel, H014 was first injected, followed by ACE2, whereas in
592 the lower panel, ACE2 was injected first and then H014. The control groups are
593 depicted by black curves. **(D)** Amount of virus on the cell surface, as detected by
594 RT-PCR. Pre-attachment mode: incubate SARS-CoV-2 and H014 first, then add the
595 mixture into cells (left); post-attachment mode: incubate SARS-CoV-2 and cells
596 first, then add H014 into virus-cell mixtures (right). High concentrations of H014
597 prevent attachment of SARS-CoV-2 to the cell surface when SARS-CoV-2 was
598 exposed to H014 before cell attachment. Values represent mean ± SD. Experiments
599 were performed in duplicates. **(E)** Clashes between H014 Fab and ACE2 upon
600 binding to SARS-CoV-2 S. H014 and ACE2 are represented as surface;
601 SARS-CoV-2 S trimer is shown as ribbon. Inset is a zoomed-in view of the
602 interactions of the RBD, H014 and ACE2 and the clashed region (oval ellipse)
603 between H014 and ACE2. The H014 Fab light and heavy chains, ACE2, and RBD
604 are presented as cartoons. The epitope, RBM and the overlapped binding region of
605 ACE2 and H014 on RBD are highlighted in green, blue and red, respectively.
606
607
608
609
610
611
612
613
614
615
616
617

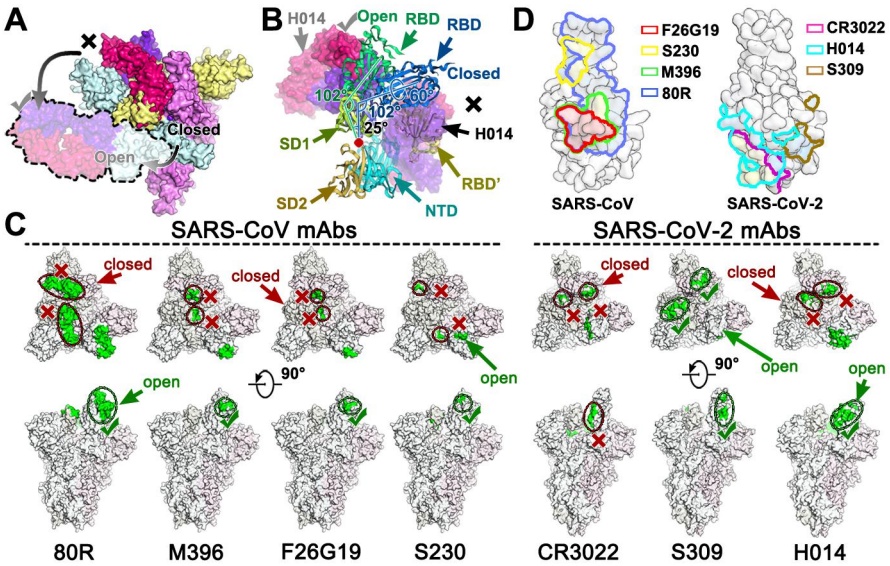

Fig. 4 Breathing of the S1 subunit and epitopes of neutralizing antibodies

(A) H014 can only interact with the "open" RBD, whereas the "closed" RBD is inaccessible to H014. The "open" RBD and RBD bound H014 are depicted in lighter colors corresponding to the protein chain they belong to. Color scheme is the same as in Fig. 2A. **(B)** Structural rearrangements of the S1 subunit of SARS-CoV-2 transition from the closed state to the open state. SD1: subdomain 1, SD2: subdomain 2, RBD': RBD (closed state) from adjacent monomer. SD1, SD2, NTD, RBD and RBD' are colored in pale green, light orange, cyan, blue and yellow, respectively. The red dot indicates the hinge point. The angles between the RBD and SD1 are labeled. **(C)** Epitope location analysis of neutralizing antibodies on SARS-CoV and SARS-CoV-2 S trimers. The S trimer structures with one RBD open and two RBD closed from SARS-CoV and SARS-CoV-2 were used to show individual epitope information, which is highlighted in green. The accessible and in-accessible states are encircled and marked by green ticks and red crosses. **(D)** Footprints of the seven mAbs on RBDs of SARS-CoV (left) and SARS-CoV-2 (right). RBDs are rendered as molecular surfaces in light blue. Footprints of different mAbs are highlighted in different colors as labeled in the graph. Note: epitopes recognized by indicated antibodies are labeled in blue (non-overlapped), yellow (overlapped once) and red (overlapped twice).